

1      **MitoChime: A Machine-Learning Pipeline for**  
2      **Detecting PCR-Induced Chimeras in**  
3      **Mitochondrial Illumina Reads**

4                          A Special Project Proposal  
5                          Presented to  
6                          the Faculty of the Division of Physical Sciences and Mathematics  
7                          College of Arts and Sciences  
8                          University of the Philippines Visayas  
9                          Miag-ao, Iloilo

10                         In Partial Fulfillment  
11                         of the Requirements for the Degree of  
12                         Bachelor of Science in Computer Science

13                         by

14                         Duranne Duran  
15                         Yvonne Lin  
16                         Daniella Pailden

17                         Adviser  
18                         Francis D. Dimzon, Ph.D.

19                         December 5, 2025

# **Contents**

21	<b>1 Introduction</b>	1
22	1.1 Overview . . . . .	1
23	1.2 Problem Statement . . . . .	3
24	1.3 Research Objectives . . . . .	4
25	1.3.1 General Objective . . . . .	4
26	1.3.2 Specific Objectives . . . . .	4
27	1.4 Scope and Limitations of the Research . . . . .	5
28	1.5 Significance of the Research . . . . .	6
29	<b>2 Review of Related Literature</b>	7
30	2.1 The Mitochondrial Genome . . . . .	7
31	2.1.1 Mitochondrial Genome Assembly . . . . .	8

32	2.2 PCR Amplification and Chimera Formation . . . . .	9
33	2.3 Existing Traditional Approaches for Chimera Detection . . . . .	10
34	2.3.1 UCHIME . . . . .	11
35	2.3.2 UCHIME2 . . . . .	12
36	2.3.3 CATch . . . . .	13
37	2.3.4 ChimPipe . . . . .	14
38	2.4 Machine Learning Approaches for Chimera and Sequence Quality	
39	Detection . . . . .	15
40	2.4.1 Feature-Based Representations of Genomic Sequences . . .	16
41	2.5 Synthesis of Chimera Detection Approaches . . . . .	18
42	<b>3 Research Methodology</b>	<b>21</b>
43	3.1 Research Activities . . . . .	21
44	3.1.1 Data Collection . . . . .	22
45	3.1.2 Bioinformatics Tools Pipeline . . . . .	26
46	3.1.3 Machine Learning Model Development . . . . .	29
47	3.1.4 Model Benchmarking, Hyperparameter Optimization, and	
48	Evaluation . . . . .	30
49	3.1.5 Feature Importance and Interpretation . . . . .	31

50	3.1.6 Validation and Testing . . . . .	32
51	3.1.7 Documentation . . . . .	33
52	3.2 Calendar of Activities . . . . .	34
53	<b>4 Results and Discussion</b>	<b>35</b>
54	4.1 Baseline Classification Performance . . . . .	35
55	4.2 Effect of Hyperparameter Tuning . . . . .	37
56	4.3 Detailed Evaluation of Representative Models . . . . .	38
57	4.3.1 Confusion Matrices and Error Patterns . . . . .	39
58	4.3.2 ROC and Precision–Recall Curves . . . . .	40

# <sup>59</sup> List of Figures

<sup>60</sup>	3.1 Process Diagram of Special Project . . . . .	22
<sup>61</sup>	4.1 Test F1 of all baseline classifiers, showing that no single model	
<sup>62</sup>	clearly dominates and several achieve comparable performance. . .	36
<sup>63</sup>	4.2 Comparison of test F1 (left) and ROC–AUC (right) for baseline and	
<sup>64</sup>	tuned models. Hyperparameter tuning yields small but consistent	
<sup>65</sup>	gains, particularly for tree-based ensembles. . . . .	38
<sup>66</sup>	4.3 Confusion matrices for the four representative models on the held-	
<sup>67</sup>	out test set. All models show more false negatives (chimeric reads	
<sup>68</sup>	called clean) than false positives. . . . .	40
<sup>69</sup>	4.4 ROC (left) and precision–recall (right) curves for the four represen-	
<sup>70</sup>	tative models on the held-out test set. Tree-based ensembles cluster	
<sup>71</sup>	closely, with logistic regression performing slightly but consistently	
<sup>72</sup>	worse. . . . .	41

# **73 List of Tables**

74	2.1 Comparison of Chimera Detection Methods . . . . .	19
75	3.1 Timetable of Activities . . . . .	34
76	4.1 Performance of baseline classifiers on the held-out test set. . . . .	36
77	4.2 Performance of tuned classifiers on the held-out test set. . . . .	37

<sup>78</sup> **Chapter 1**

<sup>79</sup> **Introduction**

<sup>80</sup> **1.1 Overview**

<sup>81</sup> The rapid advancement of next-generation sequencing (NGS) technologies has  
<sup>82</sup> transformed genomic research by enabling high-throughput and cost-effective  
<sup>83</sup> DNA analysis (Metzker, 2010). Among current platforms, Illumina sequencing  
<sup>84</sup> remains the most widely adopted, capable of producing millions of short reads  
<sup>85</sup> that can be assembled into reference genomes or analyzed for genetic variation  
<sup>86</sup> (Bentley et al., 2008; Glenn, 2011). Despite its high base-calling accuracy,  
<sup>87</sup> Illumina sequencing is prone to artifacts introduced during library preparation,  
<sup>88</sup> particularly polymerase chain reaction (PCR)-induced chimeras, which are ar-  
<sup>89</sup> tificial hybrid sequences that do not exist in the true genome (Judo, Wedel, &  
<sup>90</sup> Wilson, 1998).

<sup>91</sup> PCR chimeras form when incomplete extension products from one template

anneal to an unrelated DNA fragment and are extended, creating recombinant reads (Qiu et al., 2001). In mitochondrial genome assembly, such artifacts are especially problematic because the mitochondrial genome is small, circular, and often repetitive (Boore, 1999; Cameron, 2014). Even a small number of chimeric or misjoined reads can reduce assembly contiguity and introduce false junctions during organelle genome reconstruction (Dierckxsens, Mardulyn, & Smits, 2017; Hahn, Bachmann, & Chevreux, 2013; Jin et al., 2020). Existing assembly tools such as GetOrganelle and MITObim assume that input reads are largely free of such artifacts (Hahn et al., 2013; Jin et al., 2020). Consequently, undetected chimeras may produce fragmented assemblies or misidentified organellar boundaries. To ensure accurate reconstruction of mitochondrial genomes, a reliable method for detecting and filtering PCR-induced chimeras before assembly is essential.

This study focuses on mitochondrial sequencing data from the genus *Sardinella*, a group of small pelagic fishes widely distributed in Philippine waters. Among them, *Sardinella lemuru* (Bali sardinella) is one of the country's most abundant and economically important species, providing protein and livelihood to coastal communities (Labrador, Agmata, Palermo, Ravago-Gotanco, & Pante, 2021; Willette, Bognot, Mutia, & Santos, 2011). Accurate mitochondrial assemblies are critical for understanding its population genetics, stock structure, and evolutionary history. However, assembly pipelines often encounter errors or fail to complete due to undetected chimeric reads. To address this gap, this research introduces MitoChime, a machine learning pipeline designed to detect and filter PCR-induced chimeric reads using both alignment-based and sequence-derived statistical features. The tool aims to provide bioinformatics laboratories, partic-

117 ularly the Philippine Genome Center Visayas (PGC Visayas), with an efficient  
118 solution for improving mitochondrial genome reconstruction.

## 119 1.2 Problem Statement

120 While NGS technologies have revolutionized genomic data acquisition, the ac-  
121 curacy of mitochondrial genome assembly remains limited by artifacts produced  
122 during PCR amplification. These chimeric reads can distort assembly graphs and  
123 cause misassemblies, with particularly severe effects in small, circular mitochon-  
124 drial genomes (Boore, 1999; Cameron, 2014). Existing assembly pipelines such  
125 as GetOrganelle, MITObim, and NOVOPlasty assume that sequencing reads are  
126 free of such artifacts (Dierckxsens et al., 2017; Hahn et al., 2013; Jin et al., 2020).  
127 At PGC Visayas, several mitochondrial assemblies have failed or yielded incom-  
128 plete contigs despite sufficient coverage, suggesting that undetected chimeric reads  
129 compromise assembly reliability. Meanwhile, existing chimera detection tools such  
130 as UCHIME and VSEARCH were developed primarily for amplicon-based com-  
131 munity analysis and rely heavily on reference or taxonomic comparisons (Edgar,  
132 Haas, Clemente, Quince, & Knight, 2011; Rognes, Flouri, Nichols, Quince, &  
133 Mahé, 2016). These approaches are unsuitable for single-species organellar data,  
134 where complete reference genomes are often unavailable. Therefore, there is a  
135 pressing need for a reference-independent, data-driven tool capable of detecting  
136 and filtering PCR-induced chimeras in mitochondrial sequencing datasets.

<sup>137</sup> **1.3 Research Objectives**

<sup>138</sup> **1.3.1 General Objective**

<sup>139</sup> This study aims to develop and evaluate a machine learning-based pipeline (Mi-  
<sup>140</sup> toChime) that detects PCR-induced chimeric reads in *Sardinella lemuru* mito-  
<sup>141</sup> chondrial sequencing data in order to improve the quality and reliability of down-  
<sup>142</sup> stream mitochondrial genome assemblies.

<sup>143</sup> **1.3.2 Specific Objectives**

<sup>144</sup> Specifically, the study aims to:

- <sup>145</sup> 1. construct simulated *Sardinella lemuru* Illumina paired-end datasets contain-  
<sup>146</sup> ing both clean and PCR-induced chimeric reads,
- <sup>147</sup> 2. extract alignment-based and sequence-based features such as k-mer compo-  
<sup>148</sup> sition, junction complexity, and split-alignment counts from both clean and  
<sup>149</sup> chimeric reads,
- <sup>150</sup> 3. train, validate, and compare supervised machine-learning models for classi-  
<sup>151</sup> fying reads as clean or chimeric,
- <sup>152</sup> 4. determine feature importance and identify indicators of PCR-induced  
<sup>153</sup> chimerism,
- <sup>154</sup> 5. integrate the optimized classifier into a modular and interpretable pipeline  
<sup>155</sup> deployable on standard computing environments at PGC Visayas.

156 **1.4 Scope and Limitations of the Research**

157 This study focuses on detecting PCR-induced chimeric reads in Illumina paired-  
158 end mitochondrial sequencing data from *Sardinella lemuru*. The decision to re-  
159 strict the taxonomic scope to a single species is based on four considerations:  
160 (1) to limit interspecific variation in mitochondrial genome size, GC content, and  
161 repetitive regions so that differences in read patterns can be attributed more di-  
162 rectly to PCR-induced chimerism; (2) to align the analysis with relevant *S. lemuru*  
163 sequencing projects at PGC Visayas; (3) to take advantage of the availability of *S.*  
164 *lemuru* mitochondrial assemblies and raw datasets in public repositories such as  
165 the National Center for Biotechnology Information (NCBI), which facilitates refer-  
166 ence selection and benchmarking; and (4) to develop a tool that directly supports  
167 local studies on *S. lemuru* population structure and fisheries management.

168 The study emphasizes `wgsim`-based simulations and selected empirical mito-  
169 chondrial datasets from *S. lemuru*. It excludes naturally occurring chimeras, nu-  
170 clear mitochondrial pseudogenes (NUMTs), and large-scale assembly rearrange-  
171 ments in nuclear genomes. Feature extraction is restricted to low-dimensional  
172 alignment and sequence statistics, such as k-mer frequency profiles, GC content,  
173 read length, soft and hard clipping metrics, split-alignment counts, and map-  
174 ping quality, rather than high-dimensional deep learning embeddings. This de-  
175 sign keeps model behaviour interpretable and ensures that the pipeline can be  
176 run on standard workstations at PGC Visayas. Testing on long-read platforms  
177 (e.g., Nanopore, PacBio) and other taxa is outside the scope of this project; the  
178 implemented pipeline is evaluated only on short-read *S. lemuru* datasets.

## <sup>179</sup> 1.5 Significance of the Research

<sup>180</sup> This research provides both methodological and practical contributions to mi-  
<sup>181</sup>tochondrial genomics and bioinformatics. First, MitoChime filters PCR-induced  
<sup>182</sup> chimeric reads prior to genome assembly, with the goal of improving the con-  
<sup>183</sup>tiguity and correctness of *Sardinella lemuru* mitochondrial assemblies. Second,  
<sup>184</sup> it replaces informal manual curation with a documented workflow, improving au-  
<sup>185</sup>tomation and reproducibility. Third, the pipeline is designed to run on computing  
<sup>186</sup> infrastructures commonly available in regional laboratories, enabling routine use  
<sup>187</sup> at facilities such as PGC Visayas. Finally, more reliable mitochondrial assemblies  
<sup>188</sup> for *S. lemuru* provide a stronger basis for downstream applications in the field of  
<sup>189</sup> fisheries and genomics.

<sup>190</sup> **Chapter 2**

<sup>191</sup> **Review of Related Literature**

<sup>192</sup> This chapter presents an overview of the literature relevant to the study. It  
<sup>193</sup> discusses the biological and computational foundations underlying mitochondrial  
<sup>194</sup> genome analysis and assembly, as well as existing tools, algorithms, and techniques  
<sup>195</sup> related to chimera detection and genome quality assessment. The chapter aims to  
<sup>196</sup> highlight the strengths, limitations, and research gaps in current approaches that  
<sup>197</sup> motivate the development of the present study.

<sup>198</sup> **2.1 The Mitochondrial Genome**

<sup>199</sup> Mitochondrial genome (mtDNA) is a small, typically circular molecule found in  
<sup>200</sup> most eukaryotes. It encodes essential genes involved in oxidative phosphorylation  
<sup>201</sup> and energy metabolism. Because of its conserved structure, mtDNA has become  
<sup>202</sup> a valuable genetic marker for studies in population genetics and phylogenetics  
<sup>203</sup> (Anderson et al., 1981; Boore, 1999). In animal species, the mitochondrial genome

204 ranges from 15–20 kilobase and contains 13 protein-coding genes, 22 tRNAs, and  
205 two rRNAs arranged compactly without introns (Gray, 2012). In comparison to  
206 nuclear DNA, the ratio of the number of copies of mtDNA is higher and has  
207 simple organization which make it particularly suitable for genome sequencing  
208 and assembly studies (Dierckxsens et al., 2017).

### 209 **2.1.1 Mitochondrial Genome Assembly**

210 Mitochondrial genome assembly refers to the reconstruction of the complete mito-  
211 chondrial DNA (mtDNA) sequence from raw or fragmented sequencing reads. It is  
212 conducted to obtain high-quality, continuous representations of the mitochondrial  
213 genome that can be used for a wide range of analyses, including species identi-  
214 fication, phylogenetic reconstruction, evolutionary studies, and investigations of  
215 mitochondrial diseases. Because mtDNA evolves rapidly, its assembled sequence  
216 provides valuable insights into population structure, lineage divergence, and adap-  
217 tive evolution across taxa (Boore, 1999). Compared to nuclear genome assembly,  
218 assembling the mitochondrial genome is often considered more straightforward but  
219 still encounters technical challenges such as the formation of chimeric reads. Com-  
220 monly used tools for mitogenome assembly such as GetOrganelle and MITObim  
221 operate under the assumption of organelle genome circularity, and are vulnerable  
222 when chimeric reads disrupt this circular structure, resulting in assembly errors  
223 (Hahn et al., 2013; Jin et al., 2020).

## **224 2.2 PCR Amplification and Chimera Formation**

225 PCR plays an important role in NGS library preparation, as it amplifies target  
226 DNA fragments for downstream analysis. However as previously mentioned, the  
227 amplification process can also introduce chimeric reads which compromises the  
228 quality of the input reads supplied to sequencing or assembly workflows. Chimeras  
229 typically arise when incomplete extension occurs during a PCR cycle. This causes  
230 the DNA polymerase to switch from one template to another and generate hy-  
231 brid recombinant molecules (Judo et al., 1998). Artificial chimeras are produced  
232 through such amplification errors, whereas biological chimeras occur naturally  
233 through genomic rearrangements or transcriptional events.

234 In the context of amplicon-based sequencing, the presence of chimeras can in-  
235 flate estimates of genetic or microbial diversity and may cause misassemblies dur-  
236 ing genome reconstruction. Qin et al. (2023) has reported that chimeric sequences  
237 may account for more than 10% of raw reads in amplicon datasets. This artifact  
238 tends to be most prominent among rare operational taxonomic units (OTUs) or  
239 singletons, which are sometimes misinterpreted as novel diversity, further caus-  
240 ing the complication of microbial diversity analyses (Gonzalez, Zimmermann, &  
241 Saiz-Jimenez, 2004). As such, determining and minimizing PCR-induced chimera  
242 formation is vital for improving the quality of mitochondrial genome assemblies,  
243 and ensuring the reliability of amplicon sequencing data.

## **244 2.3 Existing Traditional Approaches for Chimera**

### **245 Detection**

**246** Several computational tools have been developed to identify chimeric sequences in  
**247** NGS datasets. These tools generally fall into two categories: reference-based and  
**248** de novo approaches. Reference-based chimera detection, also known as database-  
**249** dependent detection, is one of the earliest and most widely used computational  
**250** strategies for identifying chimeric sequences in amplicon-based community studies.  
**251** These methods rely on the comparison of each query sequence against a curated,  
**252** high-quality database of known, non-chimeric reference sequences (Edgar et al.,  
**253** 2011).

**254** On the other hand, the de novo chimera detection, also referred to as reference-  
**255** free detection, represents an alternative computational paradigm that identifies  
**256** chimeric sequences without reliance on external reference databases. This method  
**257** infer chimeras based on internal relationships among the sequences present within  
**258** the dataset itself, making it particularly advantageous in studies of under explored  
**259** or taxonomically diverse communities where comprehensive reference databases  
**260** are unavailable or incomplete (Edgar, 2016; Edgar et al., 2011). The underlying  
**261** assumption on this method is that during PCR, true biological sequences are  
**262** generally more abundant as they are amplified early and dominate the read pool,  
**263** whereas chimeric sequences appear later and are generally less abundant. The  
**264** de novo approach leverage this abundance hierarchy, treating the most abundant  
**265** sequences as supposed parents and testing whether less abundant sequences can  
**266** be reconstructed as mosaics of these templates. Compositional and structural  
**267** similarity are also evaluated to check whether different regions of a candidate

268 sequence correspond to distinct high-abundance sequences.

269 In practice, many modern bioinformatics pipelines combine both paradigms  
270 sequentially: an initial de novo step identifies dataset-specific chimeras, followed  
271 by a reference-based pass that removes remaining artifacts relative to established  
272 databases (Edgar, 2016). These two methods of detection form the foundation of  
273 tools such as UCHIME and later UCHIME2.

### 274 2.3.1 UCHIME

275 UCHIME is one of the most widely used computational tools for detecting chimeric  
276 sequences in amplicon sequencing data, as it serves as a critical quality control  
277 step to prevent the misinterpretation of PCR artifacts as novel biological diversity.  
278 The algorithm operates by searching for a model ( $M$ ) where a query ( $Q$ ) sequence  
279 can be perfectly explained as a combination of two parent sequences, denoted as  
280  $A$  and  $B$  (Edgar et al., 2011).

281 In reference mode, UCHIME divides the query into four chunks and maps  
282 them to a trusted chimeric-free database to identify candidate parents. It then  
283 constructs a three-way alignment to calculate a score based on “votes.” A “Yes”  
284 vote indicates the query aligns with parent  $A$  in one region and parent  $B$  in an-  
285 other, while a “No” vote penalizes the score if the query diverges from the expected  
286 chimeric model. In de novo mode, the algorithm operationalizes the abundance  
287 skew principle described in Section 2.3. Instead of using an external database,  
288 UCHIME dynamically treats the sample’s own high-abundance sequences as a  
289 reference database, testing if lower-abundance sequences can be reconstructed as

290 mosaics of these internal ancestors (Edgar et al., 2011).

291       Despite its high sensitivity, UCHIME has inherent limitations rooted in  
292 sequence divergence and database quality. The algorithm struggles to detect  
293 chimeras formed from parents that are very closely related, specifically when the  
294 sequence divergence between parents is less than roughly 0.8%, as the signal-to-  
295 noise ratio becomes too low to distinguish a crossover event from sequencing error  
296 (Edgar et al., 2011). Furthermore, in reference mode, the accuracy is strictly  
297 bound by the completeness of the database; if true parents are absent, the tool  
298 may fail to identify the chimera or produce false positives. Similarly, the de novo  
299 mode relies on the assumption that parents are present and sufficiently more  
300 abundant in the sample, which may not hold true in unevenly amplified samples  
301 or complex communities.

### 302       **2.3.2 UCHIME2**

303 Building upon the original algorithm, UCHIME2 was developed to address the  
304 nuances of high-resolution amplicon sequencing. A key contribution of the  
305 UCHIME2 study was the critical re-evaluation of chimera detection benchmarks.  
306 In the UCHIME2 paper (Edgar, 2016) and the UCHIME in practice website  
307 (Edgar, n.d), the author has noted that the accuracy results reported in the  
308 original UCHIME paper were “highly over-optimistic” because they relied on  
309 unrealistic benchmark designs where parent sequences were assumed to be 100%  
310 known and present. UCHIME2 introduced more rigorous testing (the CHSIMA  
311 benchmark), revealing that “fake models,” where a valid biological sequence  
312 perfectly mimics a chimera of two other valid sequences, are far more common

than previously assumed. This discovery suggests that error-free detection is impossible in principle (Edgar, 2016). Another notable improvement is the introduction of multiple application-specific modes that allow users to tailor the algorithm’s performance to the characteristics of their datasets. The following parameter presets: denoised, balanced, sensitive, specific, and high-confidence, enable researchers to optimize the balance between sensitivity and specificity according to the goals of their analysis.

However despite these advancements, the practical application of UCHIME2 requires caution. The author explicitly advises against using UCHIME2 as a stand-alone tool in standard OTU clustering or denoising pipelines. Using UCHIME2 as an independent filtering step in these workflows is discouraged, as it often results in significantly higher error rates, increasing both false positives (discarding valid sequences) and false negatives (retaining chimeras) (Edgar, 2016).

### 2.3.3 CATch

As previously mentioned, UCHIME (Edgar et al., 2011) relied on alignment-based sequences in amplicon data. However, researchers soon observed that different algorithms often produced inconsistent predictions. A sequence might be identified as chimeric by one tool but classified as non-chimeric by another, resulting in unreliable filtering outcomes across studies.

To address these inconsistencies, Mysara, Saeys, Leys, Raes, and Monsieurs (2015) developed the Classifier for Amplicon Tool Chimeras (CATCh), which rep-

335 resents the first ensemble machine learning system designed for chimera detection  
336 in 16S rRNA amplicon sequencing. Rather than depending on a single detec-  
337 tion strategy, CATCh integrates the outputs of several established tools, includ-  
338 ing UCHIME, ChimeraSlayer, DECIPHER, Pintail, and Perseus. The individual  
339 scores and binary decisions generated by these tools are used as input features for  
340 a supervised learning model. The algorithm employs a Support Vector Machine  
341 (SVM) with a Pearson VII Universal Kernel (PUK) to determine optimal weight-  
342 ings among the input features and to assign each sequence a probability of being  
343 chimeric.

344 Benchmarking in both reference-based and de novo modes demonstrated signif-  
345 icant performance improvements. CATCh achieved sensitivities of approximately  
346 85 percent in reference-based mode and 92 percent in de novo mode, with corre-  
347 sponding specificities of approximately 96 percent and 95 percent. These results  
348 indicate that CATCh detected 7 to 12 percent more chimeras than any individual  
349 algorithm while maintaining high precision.

### 350 2.3.4 ChimPipe

351 Among the available tools for chimera detection, ChimPipe is a pipeline developed  
352 to identify chimeric sequences such as biological chimeras. It uses both discordant  
353 paired-end reads and split-read alignments to improve the accuracy and sensitivity  
354 of detecting biological chimeras (Rodriguez-Martin et al., 2017). By combining  
355 these two sources of information, ChimPipe achieves better precision than meth-  
356 ods that depend on a single type of indicator.

357        The pipeline works with many eukaryotic species that have available genome  
358        and annotation data (Rodriguez-Martin et al., 2017). It can also predict multiple  
359        isoforms for each gene pair and identify breakpoint coordinates that are useful  
360        for reconstructing and verifying chimeric transcripts. Tests using both simulated  
361        and real datasets have shown that ChimPipe maintains high accuracy and reliable  
362        performance.

363        ChimPipe lets users adjust parameters to fit different sequencing protocols or  
364        organism characteristics. Experimental results have confirmed that many chimeric  
365        transcripts detected by the tool correspond to functional fusion proteins, demon-  
366        strating its utility for understanding chimera biology and its potential applications  
367        in disease research (Rodriguez-Martin et al., 2017).

## 368        **2.4 Machine Learning Approaches for Chimera 369                          and Sequence Quality Detection**

370        Traditional chimera detection tools rely primarily on heuristic or alignment-based  
371        rules. Recent advances in machine learning (ML) have demonstrated that models  
372        trained on sequence-derived features can effectively capture compositional and  
373        structural patterns in biological sequences. Although most existing ML systems  
374        such as those used for antibiotic resistance prediction, taxonomic classification,  
375        or viral identification are not specifically designed for chimera detection, they  
376        highlight how data-driven models can outperform similarity-based heuristics by  
377        learning intrinsic sequence signatures. In principle, ML frameworks can integrate  
378        indicators such as k-mer frequencies, GC-content variation and split-alignment

379 metrics to identify subtle anomalies that may indicate a chimeric origin (Arango  
380 et al., 2018; Liang, Bible, Liu, Zou, & Wei, 2020; Ren et al., 2020).

381 **2.4.1 Feature-Based Representations of Genomic Se-**  
382 **quences**

383 In genomic analysis, feature extraction converts DNA sequences into numerical  
384 representations suitable for ML algorithms. A common approach is k-mer fre-  
385 quency analysis, where normalized k-mer counts form the feature vector (Vervier,  
386 Mahé, Tournoud, Veyrieras, & Vert, 2015). These features effectively capture lo-  
387 cal compositional patterns that often differ between authentic and chimeric reads.

388 In particular, deviations in k-mer profiles between adjacent read segments can  
389 serve as a compositional signature of template-switching events. Additional de-  
390 scriptors such as GC content and sequence entropy can further distinguish se-  
391 quence types; in metagenomic classification and virus detection, k-mer-based fea-  
392 tures have shown strong performance and robustness to noise (Ren et al., 2020;  
393 Vervier et al., 2015). For chimera detection specifically, abrupt shifts in GC or k-  
394 mer composition along a read can indicate junctions between parental fragments.  
395 Windowed feature extraction enables models to capture these discontinuities that  
396 rule-based algorithms may overlook.

397 Machine learning models can also leverage alignment-derived features such as  
398 the frequency of split alignments, variation in mapping quality, and local cover-  
399 age irregularities. Split reads and discordant read pairs are classical indicators  
400 of genomic junctions and have been formalized in probabilistic frameworks for  
401 structural-variant discovery that integrate multiple evidence types (Layer, Hall, &

402 Quinlan, 2014). Similarly, long-read tools such as Sniffles employ split-alignment  
403 and coverage anomalies to accurately localize breakpoints (Sedlazeck et al., 2018).  
404 Modern aligners such as Minimap2 (Li, 2018) output supplementary (SA tags) and  
405 secondary alignments as well as chaining and alignment-score statistics that can  
406 be summarized into quantitative predictors for machine-learning models. These  
407 alignment-signal features are particularly relevant to PCR-induced mitochondrial  
408 chimeras, where template-switching events produce reads partially matching dis-  
409 tinct regions of the same or related genomes. Integrating such cues within a  
410 supervised-learning framework enables artifact detection even in datasets lacking  
411 complete or perfectly assembled references.

412 A further biologically grounded descriptor is the length of microhomology at  
413 putative junctions. Microhomology refers to short, shared sequences, often in the  
414 range of a few to tens of base pairs that are near breakpoints where template-  
415 switching events typically happen. Studies of double strand break repair and  
416 structural variation have demonstrated that the length of microhomology corre-  
417 lates with the likelihood of microhomology-mediated end joining (MMEJ) or fork-  
418 stalled template-switching pathways (Sfeir & Symington, 2015). In the context of  
419 PCR-induced chimeras, template switching during amplification often leaves short  
420 identical sequences at the junction of two concatenated fragments. Quantifying  
421 the longest exact suffix–prefix overlap at each candidate breakpoint thus provides  
422 a mechanistic signature of chimerism and complements both compositional (k-  
423 mer) and alignment (SA count) features.

## **424 2.5 Synthesis of Chimera Detection Approaches**

<sup>425</sup> To provide an integrated overview of the literature discussed in this chapter, Ta-  
<sup>426</sup> ble 2.1 summarizes the major chimera detection studies, their methodological  
<sup>427</sup> approaches, and their known limitations.

Table 2.1: Comparison of Chimera Detection Methods

Methods	Approach	Limitations
<b>Reference-based Chimera Detection</b>	Compares query sequences against curated, non-chimeric reference databases; identifies mosaic sequences by evaluating similarity to known templates.	Depends heavily on completeness and quality of reference databases; often fails when novel taxa or missing parent sequences are present; reduced accuracy for low-divergence chimeras.
<b>De novo Chimera Detection</b>	Identifies chimeras using only internal dataset relationships; relies on abundance patterns and compositional similarity; reconstructs sequences as mosaics of high-abundance parents.	Assumes true sequences are more abundant—fails when amplification bias distorts abundance; struggles with evenly abundant parental sequences; can misclassify highly similar true variants.
<b>UCHIME</b>	Alignment-based chimera detection; segments query sequence, identifies parent candidates, performs 3-way alignment, and computes chimera scores; supports both reference-based and de novo modes.	Accuracy inflated in original benchmarks; suffers under incomplete databases; poor performance on low-divergence chimeras; sensitive to sequencing errors; misclassifies when parents are missing.
<b>UCHIME2</b>	Improved initial UCHIME benchmarking; offers multiple sensitivity/specificity modes; more robust with incomplete references; higher sensitivity.	Cannot achieve perfect accuracy due to “perfect fake models”; genuine variants may be indistinguishable from artificial recombinants; theoretical detection limit remains.
<b>CATCh</b>	First ML ensemble tool for 16S chimera detection; integrates outputs of UCHIME, ChimeraSlayer, DECIPHER, Pintail, Perseus via SVM classifier; significantly improves sensitivity and specificity.	Depends on performance of underlying tools; ML model limited to features they output; ensemble can still misclassify in datasets with extreme novelty or low coverage.
<b>ChimPipe</b>	Pipeline for detecting fusion genes and transcript-derived chimeras in RNA-seq; uses discordant paired-end reads and split-alignments; predicts isoforms and breakpoint coordinates.	Designed for RNA-seq, not amplicons; needs high-quality genome and annotation; computationally heavier; limited to organisms with reference genomes.

428 Across existing studies, no single approach reliably detects all forms of chimeric  
429 sequences, particularly those generated by PCR-induced template switching in  
430 mitochondrial genomes. Reference-based tools perform poorly when parental se-  
431 quences are absent; de novo methods rely strongly on abundance assumptions;  
432 alignment-based systems show reduced sensitivity to low-divergence chimeras; and  
433 ensemble methods inherit the limitations of their component algorithms. RNA-  
434 seq-oriented pipelines likewise do not generalize well to organelle data. Although  
435 machine learning approaches offer promising feature-based detection, they are  
436 rarely applied to mitochondrial genomes and are not trained specifically on PCR-  
437 induced organelle chimeras. These limitations indicate a clear research gap: the  
438 need for a specialized, feature-driven classifier tailored to mitochondrial PCR-  
439 induced chimeras that integrates k-mer composition, split-alignment signals, and  
440 micro-homology features to achieve more accurate detection than current heuristic  
441 or alignment-based tools.

# <sup>442</sup> Chapter 3

## <sup>443</sup> Research Methodology

<sup>444</sup> This chapter outlines the steps involved in completing the study, including data  
<sup>445</sup> gathering, generating simulated mitochondrial Illumina reads, preprocessing and  
<sup>446</sup> indexing the data, developing a bioinformatics pipeline to extract key features,  
<sup>447</sup> applying machine learning algorithms for chimera detection, and validating and  
<sup>448</sup> comparing model performance.

### <sup>449</sup> 3.1 Research Activities

<sup>450</sup> As illustrated in Figure 3.1, this study carried out a sequence of procedures to  
<sup>451</sup> detect PCR-induced chimeric reads in mitochondrial genomes. The process began  
<sup>452</sup> with collecting a mitochondrial reference sequence of *Sardinella lemuru* from the  
<sup>453</sup> National Center for Biotechnology Information (NCBI) database, which was used  
<sup>454</sup> as a reference for generating simulated clean and chimeric reads. These reads  
<sup>455</sup> were subsequently indexed and mapped. The resulting collections then passed

456 through a bioinformatics pipeline that extracted k-mer profiles, supplementary  
457 alignment (SA) features, and microhomology information to prepare the data for  
458 model construction. The machine learning model was trained using the processed  
459 input, and its precision and accuracy were assessed. It underwent tuning until it  
460 reached the desired performance threshold, after which it proceeded to validation  
461 and will undergo testing.

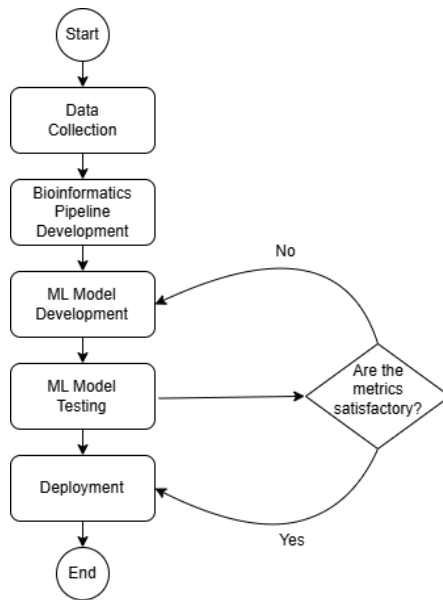


Figure 3.1: Process Diagram of Special Project

### 462 3.1.1 Data Collection

463 The mitochondrial genome reference sequence of *S. lemuru* was obtained from the  
464 NCBI database (accession number NC\_039553.1) in FASTA format. This sequence  
465 served as the basis for generating simulated reads for model development.

466 This step was scheduled to begin in the first week of November 2025 and  
467 expected to be completed by the end of that week, with a total duration of ap-

468 proximately one (1) week.

469 **Data Preprocessing**

470 To reduce manual repetition, all steps in the simulation and preprocessing pipeline  
471 were executed using a custom script in Python (Version 3.11). The script runs  
472 each stage, including read simulation, reference indexing, mapping, and alignment  
473 processing, in a fixed sequence.

474 Sequencing data were simulated from the NCBI reference genome using `wgsim`  
475 (Version 1.13). First, a total of 10,000 paired-end fragments were simulated,  
476 producing 20,000 reads (10,000 forward and 10,000 reverse) from the the original  
477 reference (`original_reference.fasta`) and and designated as clean reads using  
478 the command:

```
479 wgsim -1 150 -2 150 -r 0 -R 0 -X 0 -e 0.001 -N 10000 \  
480           original_reference.fasta ref1.fastq ref2.fastq
```

481 The command parameters are as follows:

- 482 • `-1` and `-2`: read lengths of 150 base pairs for each paired-end read.
- 483 • `-r`, `-R`, `-X`: mutation rate, fraction of indels, and indel extension probability,  
484 all set to a default value of 0.
- 485 • `-e`: base error rate, set to 0.001 to simulate realistic sequencing errors.
- 486 • `-N`: number of read pairs, set to 10,000.

487 Chimeric sequences were then generated from the same NCBI reference using a  
488 separate Python script. Two non-adjacent segments were randomly selected such  
489 that their midpoint distances fell within specified minimum and maximum thresh-  
490 olds. The script attempts to retain microhomology, or short identical sequences  
491 at segment junctions, to mimic PCR-induced template switching. The resulting  
492 chimeras were written to `chimera_reference.fasta`, with headers recording seg-  
493 ment positions and microhomology length. The `chimera_reference.fasta` was  
494 processed with `wgsim` to simulate 10,000 paired-end fragments, generating 20,000  
495 chimeric reads (10,000 forward reads in `chimeric1.fastq` and 10,000 reverse reads  
496 in `chimeric2.fastq`) using the command format.

497 Next, a `minimap2` index of the reference genome was created using:

```
498 minimap2 -d ref.mmi original_reference.fasta
```

499 Minimap2 (Version 2.28) is a tool used to map reads to a reference genome.  
500 The index `ref.mmi` of the original reference sequence is required by `minimap2` for  
501 efficient read mapping. Mapping allows extraction of alignment features from each  
502 read, which were used as input for the machine learning model. The simulated  
503 clean and chimeric reads were then mapped to the reference index as follows:

```
504 minimap2 -ax sr -t 8 ref.mmi ref1.fastq ref2.fastq > clean.sam
```

```
505 minimap2 -ax sr -t 8 ref.mmi \  
506 chimeric1.fastq chimeric2.fastq > chimeric.sam
```

507 Here, `-ax sr` specifies short-read alignment mode, and `-t 8` uses 8 CPU

508 threads. The resulting clean and chimeric SAM files contain the alignment posi-  
509 tions of each read relative to the original reference genome.

510 The SAM files were then converted to BAM format, sorted, and indexed using

511 `samtools` (Version 1.20):

```
512 samtools view -bS clean.sam -o clean.bam  
513 samtools view -bS chimeric.sam -o chimeric.bam  
514  
515 samtools sort clean.bam -o clean.sorted.bam  
516 samtools index clean.sorted.bam  
517  
518 samtools sort chimeric.bam -o chimeric.sorted.bam  
519 samtools index chimeric.sorted.bam
```

520 BAM files are the compressed binary version of SAM files, which enables faster  
521 processing and reduced storage. Sorting arranges reads by genomic coordinates,  
522 and indexing allows detection of SA as a feature for the machine learning model.

523 The total number of simulated reads was expected to be 40,000. The final col-  
524 lection of reads contained 19,984 clean reads and 20,000 chimeric reads (39,984 en-  
525 tries in total), providing a roughly balanced distribution between the two classes.  
526 After alignment with `minimap2`, only 19,984 clean reads remained because un-  
527 mapped reads were not included in the BAM file. Some sequences failed to align  
528 due to the 5% error rate defined during `wgsim` simulation, which produced mis-  
529 matches that caused certain reads to fall below the aligner's matching threshold.

530 This whole process is scheduled to start in the second week of November 2025

531 and is expected to be completed by the last week of November 2025, with a total  
532 duration of approximately three (3) weeks.

### 533 **3.1.2 Bioinformatics Tools Pipeline**

534 A bioinformatics pipeline will be developed and implemented to extract the neces-  
535 sary analytical features. This pipeline will function as a reproducible and modular  
536 workflow that accepts FASTQ and BAM/SAM file inputs, processes them using  
537 tools such as `samtools` and `jellyfish` (Version 2.3.1), and produces tabular fea-  
538 ture matrices (TSV) for downstream machine learning. To ensure correctness  
539 and adherence to best practices, bioinformatics experts at the PGC Visayas will  
540 be consulted to validate the pipeline design, feature extraction logic, and overall  
541 data integrity. This stage of the study is scheduled to begin in the first week of  
542 January 2026 and conclude by the last week of February 2026, with an estimated  
543 total duration of approximately two (2) months.

544 The bioinformatics pipeline focuses on three principal features from the simu-  
545 lated and aligned sequencing data: (1) supplementary alignment flag (SA count),  
546 (2) k-mer composition difference between read segments, and (3) microhomology  
547 length at potential junctions. Each of these features captures a distinct biological  
548 or computational signature associated with PCR-induced chimeras.

#### 549 **Supplementary Alignment Flag**

550 Supplementary alignment information will be assessed using the mapped and  
551 sorted BAM files (`clean.sorted.bam` and `chimeric.sorted.bam`) generated

552 from the data preprocessing stage. Alignment summaries will be checked using  
553 `samtools flagstat` to obtain preliminary quality-control statistics, including  
554 counts of primary, secondary, and supplementary (SA) alignments.

555 Both BAM files will be converted to SAM format for detailed inspection of  
556 reads in each file:

```
557 samtools view -h clean.sorted.bam -o clean.sorted.sam  
558 samtools view -h chimeric.sorted.bam -o chimeric.sorted.sam
```

559 The SAM output will be checked for reads containing the SA:Z flag, as it  
560 denotes supplementary alignments. Reads exhibiting these or substantial soft-  
561 clipped regions will be considered strong candidates for chimeric artifacts. A  
562 custom Python script would be created to extract the alignment-derived features  
563 and relevant metadata including mapping quality, SAM flag information, CIGAR-  
564 based clipping, and alignment coordinates. These extracted attributes would then  
565 be organized and compiled into a TSV (`.tsv`) file.

## 566 K-mer Composition Difference

567 Chimeric reads often comprise fragments from distinct genomic regions, resulting  
568 in a compositional discontinuity between segments. Comparing k-mer frequency  
569 profiles between the left and right halves of a read allows detection of such abrupt  
570 compositional shifts, independent of alignment information. This will be obtained  
571 using Jellyfish, a fast k-mer counting software. For each read, the sequence will  
572 be divided into two segments, either at the midpoint or at empirically determined  
573 breakpoints inferred from supplementary alignment data, to generate left and right

574 sequence segments. Jellyfish will then compute k-mer frequency profiles (with  $k =$   
575 5 or 6) for each segment. The resulting k-mer frequency vectors will be normalized  
576 and compared using distance metrics such as cosine similarity or Jensen–Shannon  
577 divergence to quantify compositional disparity between the two halves of the same  
578 read. The resulting difference scores will be stored in a structured TSV file.

## 579 Microhomology Length

580 The microhomology length was computed as part of the bioinformatics pipeline.  
581 For each aligned read in the BAM files, the script first inferred a breakpoint  
582 using the function `infer_breakpoint`, which represents a junction between two  
583 segments. Breakpoints were determined primarily from soft-clipping patterns.  
584 If no soft clips were present, SA tags were used to identify potential alignment  
585 discontinuities.

586 Once a breakpoint was established, the script scanned a  $\pm 40$  base pair window  
587 surrounding the breakpoint and used the function `longest_suffix_prefix_overlap`  
588 to identify the longest exact suffix-prefix overlap between the left and right read  
589 segments. This overlap, which represents consecutive bases shared at the junc-  
590 tion, was recorded as the microhomology length. Additionally, the GC content  
591 of the overlapping sequence was calculated using the function `gc_content`, which  
592 counts guanine (G) and cytosine (C) bases within the detected microhomology  
593 and divides by the total length, yielding a proportion between 0 and 1.

594 Short microhomologies, typically 3-20 base pairs in length, are recognized sig-  
595 natures of PCR-induced template switching and can promote template recombi-  
596 nation (Peccoud et al., 2018). Each read was annotated after capturing both the

597 length and GC content of microhomology.

### 598 3.1.3 Machine Learning Model Development

599 After feature extraction, the per-read feature matrices for clean and chimeric  
600 reads were merged into a single dataset. Each row corresponded to one paired-  
601 end read, and columns encoded alignment-structure features (e.g., supplementary  
602 alignment count and spacing between segments), CIGAR-derived soft-clipping  
603 statistics (e.g., left and right soft-clipped length, total clipped bases), k-mer com-  
604 position discontinuity between read segments, and microhomology descriptors  
605 near candidate junctions. The resulting feature set was restricted to quantities  
606 that can be computed from standard BAM/FASTQ files in typical mitochondrial  
607 sequencing workflows.

608 The labelled dataset was randomly partitioned into training (80%) and test  
609 (20%) subsets using stratified sampling to preserve the 1:1 ratio of clean to  
610 chimeric reads. Model development and evaluation were implemented in Python  
611 (Version 3.11) using the `scikit-learn`, `xgboost`, `lightgbm`, and `catboost` li-  
612 braries. A broad panel of classification algorithms was then benchmarked on the  
613 training data to obtain a fair comparison of different model families under identical  
614 feature conditions. The panel included: a trivial dummy classifier, L2-regularized  
615 logistic regression, a calibrated linear support vector machine (SVM),  $k$ -nearest  
616 neighbours, Gaussian Naïve Bayes, decision-tree ensembles (Random Forest, Ex-  
617 tremely Randomized Trees, and Bagging with decision trees), gradient boosting  
618 methods (Gradient Boosting, XGBoost, LightGBM, and CatBoost), and a shallow  
619 multilayer perceptron (MLP).

620 For each model, five-fold stratified cross-validation was performed on the train-  
621 ing set. In every fold, four-fifths of the data were used for fitting and the remaining  
622 one-fifth for validation. Mean cross-validation accuracy, precision, recall, F1-score  
623 for the chimeric class, and area under the receiver operating characteristic curve  
624 (ROC–AUC) were computed to summarize performance and rank candidate meth-  
625 ods. This baseline screen allowed comparison of linear, probabilistic, neural, and  
626 ensemble-based approaches and identified tree-based ensemble and boosting mod-  
627 els as consistently strong performers relative to simpler baselines.

628 **3.1.4 Model Benchmarking, Hyperparameter Optimiza-  
629 tion, and Evaluation**

630 Model selection and refinement proceeded in two stages. First, the cross-validation  
631 results from the broad panel were used to identify a subset of competitive mod-  
632 els for more detailed optimization. Specifically, ten model families were carried  
633 forward: L2-regularized logistic regression, calibrated linear SVM, Random For-  
634 est, ExtraTrees, Gradient Boosting, XGBoost, LightGBM, CatBoost, Bagging  
635 with decision trees, and a shallow MLP. This subset spans both linear and non-  
636 linear decision boundaries, but emphasizes ensemble and boosting methods, which  
637 showed superior F1 and ROC–AUC in the initial benchmark.

638 Second, hyperparameter optimization was conducted for each of the ten se-  
639 lected models using randomized search with five-fold stratified cross-validation  
640 (`RandomizedSearchCV`). For tree-based ensembles, the search space included the  
641 number of trees, maximum depth, minimum samples per split and leaf, and the  
642 fraction of features considered at each split. For boosting methods, key hyper-

643 parameters such as the number of boosting iterations, learning rate, tree depth,  
644 subsampling rate, and column subsampling rate were tuned. For the MLP, the  
645 number and size of hidden layers, learning rate, and  $L_2$  regularization strength  
646 were varied. In all cases, the primary optimisation criterion was the F1-score of  
647 the chimeric class, averaged across folds.

648 For each model family, the hyperparameter configuration with the highest  
649 mean cross-validation F1-score was selected as the best-tuned estimator. These  
650 tuned models were then refitted on the full training set and evaluated once on the  
651 held-out test set to obtain unbiased estimates of performance. Test-set metrics in-  
652 cluded accuracy, precision, recall, F1-score for the chimeric class, and ROC–AUC.  
653 Confusion matrices and ROC curves were generated for the top-performing mod-  
654 els to characterise common error modes, such as false negatives (missed chimeric  
655 reads) and false positives (clean reads incorrectly labelled as chimeric). The final  
656 model or small set of models for downstream interpretation was chosen based on  
657 a combination of test-set F1-score, ROC–AUC, and practical considerations such  
658 as model complexity and ease of deployment within a bioinformatics pipeline.

### 659 3.1.5 Feature Importance and Interpretation

660 To relate model decisions to biologically meaningful signals, feature-importance  
661 analyses were performed on the best-performing tree-based models. Two comple-  
662 mentary approaches were used. First, built-in importance measures from ensemble  
663 methods (e.g., split-based importances in Random Forest and Gradient Boosting)  
664 were examined to obtain an initial ranking of features based on their contribution  
665 to reducing impurity. Second, model-agnostic permutation importance was com-

666 puted on the test set by repeatedly permuting each feature column while keeping  
667 all others fixed and measuring the resulting decrease in F1-score. Features whose  
668 permutation led to a larger performance drop were interpreted as more influential  
669 for chimera detection.

670 For interpretability, individual features were grouped into four conceptual  
671 families: (i) supplementary alignment and alignment-structure features (e.g., SA  
672 count, spacing between alignment segments, strand consistency), (ii) CIGAR-  
673 derived soft-clipping features (e.g., left and right soft-clipped length, total clipped  
674 bases), (iii) k-mer composition discontinuity features (e.g., cosine distance and  
675 Jensen–Shannon divergence between k-mer profiles of read segments), and (iv) mi-  
676 crohomology descriptors (e.g., microhomology length and local GC content around  
677 putative breakpoints). Aggregating permutation importance scores within each  
678 family allowed assessment of which biological signatures contributed most strongly  
679 to the classifier’s performance. This analysis provided a basis for interpreting the  
680 trained models in terms of known mechanisms of PCR-induced template switching  
681 and for identifying which alignment- and sequence-derived cues are most informa-  
682 tive for distinguishing chimeric from clean mitochondrial reads.

### 683 3.1.6 Validation and Testing

684 Validation will involve both internal and external evaluations. Internal valida-  
685 tion was achieved through five-fold cross-validation on the training data to verify  
686 model generalization and reduce variance due to random sampling. External vali-  
687 dation will be achieved through testing on the 20% hold-out dataset derived from  
688 the simulated reads, which will be an unbiased benchmark to evaluate how well

689 the trained models generalized to unseen data. All feature extraction and pre-  
690 processing steps were performed using the same bioinformatics pipeline to ensure  
691 consistency and comparability across validation stages.

692 Comparative evaluation was performed across all candidate algorithms, in-  
693 cluding a trivial dummy classifier, L2-regularized logistic regression, a calibrated  
694 linear SVM, k-nearest neighbours, Gaussian Naïve Bayes, decision-tree ensembles,  
695 gradient boosting methods, and a shallow MLP. This evaluation determined which  
696 models demonstrated the highest predictive performance and computational effi-  
697 ciency under identical data conditions. Their metrics were compared to identify  
698 which algorithms were most suitable for further refinement.

### 699 **3.1.7 Documentation**

700 Comprehensive documentation was maintained throughout the study to ensure  
701 transparency and reproducibility. All stages of the research, including data gath-  
702 ering, preprocessing, feature extraction, model training, and validation, were sys-  
703 tematically recorded in a `.README` file in the GitHub repository. For each ana-  
704 lytical step, the corresponding parameters, software versions, and command line  
705 scripts were documented to enable exact replication of results.

706 The repository structure followed standard research data management prac-  
707 tices, with clear directories for datasets and scripts. Computational environments  
708 were standardized using Conda, with an environment file (`environment.arm.yml`)  
709 specifying dependencies and package versions to maintain consistency across sys-  
710 tems.

<sup>711</sup> For manuscript preparation and supplementary materials, Overleaf (L<sup>A</sup>T<sub>E</sub>X)  
<sup>712</sup> was used to produce publication-quality formatting and consistent referencing. f

## <sup>713</sup> 3.2 Calendar of Activities

<sup>714</sup> Table 3.1 presents the project timeline in the form of a Gantt chart, where each  
<sup>715</sup> bullet point corresponds to approximately one week of planned activity.

Table 3.1: Timetable of Activities

Activities (2025)	Nov	Dec	Jan	Feb	Mar	Apr	May
Data Collection and Simulation	• • •						
Bioinformatics Tools Pipeline			• • •	• • •			
Machine Learning Development			• •	• • •	• • •	• •	
Testing and Validation						• •	• • •
Documentation	• • •	• • •	• • •	• • •	• • •	• • •	• • •

# <sup>716</sup> Chapter 4

## <sup>717</sup> Results and Discussion

### <sup>718</sup> 4.1 Baseline Classification Performance

<sup>719</sup> Table 4.1 summarises the performance of eleven classifiers trained on the engi-  
<sup>720</sup> neered feature set using five-fold cross-validation and evaluated on the held-out  
<sup>721</sup> test set. All models were optimised using default hyperparameters, without ded-  
<sup>722</sup> icated tuning.

<sup>723</sup> The dummy baseline, which always predicts the same class regardless of the  
<sup>724</sup> input features, achieved an accuracy of 0.50 and test F1-score of 0.67. This re-  
<sup>725</sup> flects the balanced class distribution and provides a lower bound for meaningful  
<sup>726</sup> performance.

<sup>727</sup> Across other models, test F1-scores clustered in a narrow band between ap-  
<sup>728</sup> proximately 0.74 and 0.77 and ROC–AUC values between 0.82 and 0.84. Gradi-  
<sup>729</sup> ent boosting, CatBoost, LightGBM, XGBoost, bagging trees, random forest, and

730 multilayer perceptron (MLP) all produced very similar scores, with CatBoost and  
 731 gradient boosting slightly ahead (test F1  $\approx 0.77$ , ROC–AUC  $\approx 0.84$ ). Linear  
 732 models (logistic regression and calibrated linear SVM) performed only marginally  
 733 worse (test F1  $\approx 0.74$ ), while Gaussian Naive Bayes lagged behind with substan-  
 734 tially lower F1 ( $\approx 0.65$ ) despite very high precision for the chimeric class.

Table 4.1: Performance of baseline classifiers on the held-out test set.

model	test_accuracy	test_precision	test_recall	test_f1	test_roc_auc
dummy_baseline	0.500000	0.500000	1.000000	0.667000	0.500000
logreg_l2	0.789000	0.945000	0.614000	0.744000	0.821000
linear_svm_calibrated	0.789000	0.945000	0.614000	0.744000	0.820000
random_forest	0.788000	0.894000	0.654000	0.755000	0.834000
extra_trees	0.788000	0.901000	0.647000	0.753000	0.824000
gradient_boosting	0.802000	0.936000	0.648000	0.766000	0.840000
xgboost	0.800000	0.929000	0.650000	0.765000	0.839000
lightgbm	0.799000	0.926000	0.650000	0.764000	0.838000
catboost	0.803000	0.936000	0.650000	0.767000	0.839000
knn	0.782000	0.892000	0.642000	0.747000	0.815000
gaussian_nb	0.741000	0.996000	0.483000	0.651000	0.819000
bagging_trees	0.792000	0.900000	0.657000	0.760000	0.837000
mlp	0.789000	0.931000	0.625000	0.748000	0.819000

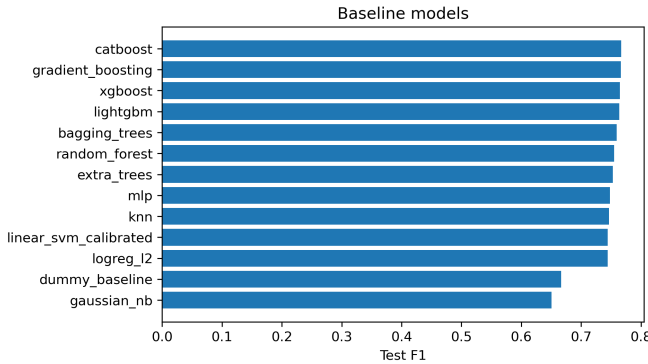


Figure 4.1: Test F1 of all baseline classifiers, showing that no single model clearly dominates and several achieve comparable performance.

## 735 4.2 Effect of Hyperparameter Tuning

736 To assess whether performance could be improved further, ten model families un-  
737 derwent randomised hyperparameter search (Chapter 3). The tuned metrics are  
738 summarised in Table 4.2. Overall, tuning yielded modest but consistent gains for  
739 tree-based ensembles and boosting methods, while leaving linear models essen-  
740 tially unchanged or slightly worse.

741 CatBoost, gradient boosting, LightGBM, XGBoost, random forest, bagging  
742 trees, and MLP all experienced small increases in test F1 (typically  $\Delta F1 \approx 0.002$ –  
743  $0.009$ ) and ROC–AUC (up to  $\Delta AUC \approx 0.008$ ). After tuning, CatBoost remained  
744 the best performer with test accuracy 0.802, precision 0.924, recall 0.658, F1-score  
745 0.769, and ROC–AUC 0.844. Gradient boosting achieved almost identical perfor-  
746 mance (F1 0.767, AUC 0.843). Random forest and bagging trees also improved  
747 to F1 scores around 0.763 with AUC  $\approx 0.842$ .

Table 4.2: Performance of tuned classifiers on the held-out test set.

model	test_accuracy	test_precision	test_recall	test_f1	test_roc_auc
logreg_l2_tuned	0.788000	0.946000	0.612000	0.743000	0.818000
linear_svm_calibrated_tuned	0.788000	0.944000	0.612000	0.743000	0.818000
random_forest_tuned	0.797000	0.915000	0.655000	0.763000	0.842000
extra_trees_tuned	0.794000	0.910000	0.652000	0.760000	0.837000
gradient_boosting_tuned	0.802000	0.928000	0.654000	0.767000	0.843000
xgboost_tuned	0.799000	0.922000	0.653000	0.765000	0.839000
lightgbm_tuned	0.801000	0.930000	0.651000	0.766000	0.842000
catboost_tuned	0.802000	0.924000	0.658000	0.769000	0.844000
bagging_trees_tuned	0.798000	0.922000	0.650000	0.763000	0.842000
mlp_tuned	0.790000	0.934000	0.625000	0.749000	0.821000

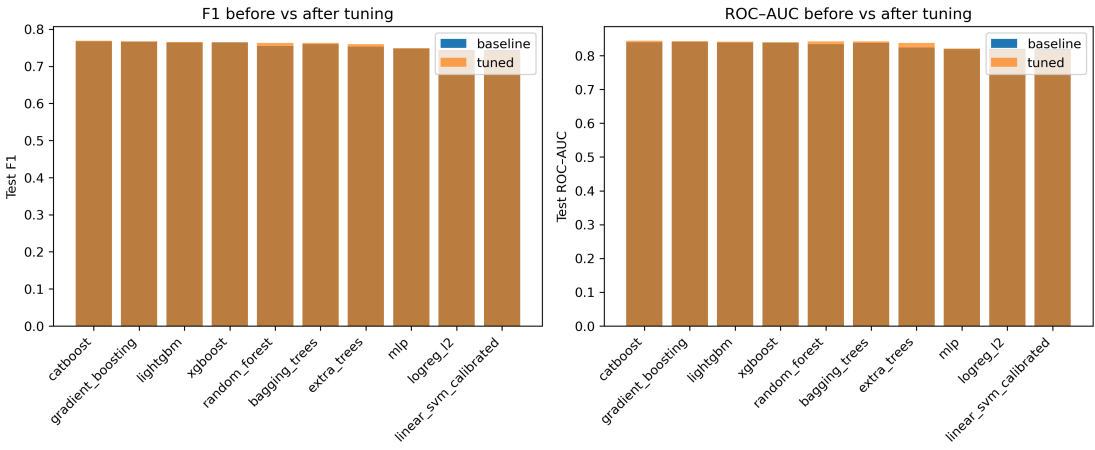


Figure 4.2: Comparison of test F1 (left) and ROC–AUC (right) for baseline and tuned models. Hyperparameter tuning yields small but consistent gains, particularly for tree-based ensembles.

748     Because improvements are small and within cross-validation variability, we  
 749     interpret tuning as stabilising and slightly refining the models rather than funda-  
 750     mentally altering their behaviour or their relative ranking.

### 751     4.3 Detailed Evaluation of Representative Mod- 752       els

753     For interpretability and diversity, four tuned models were selected for deeper  
 754     analysis: CatBoost (best-performing boosted tree), scikit-learn gradient boost-  
 755     ing (canonical gradient-boosting implementation), random forest (non-boosted  
 756     ensemble baseline), and L2-regularised logistic regression (linear baseline). All  
 757     models were trained on the engineered feature set and evaluated on the same  
 758     held-out test data.

### 759 4.3.1 Confusion Matrices and Error Patterns

760 Classification reports and confusion matrices for the four models reveal consistent  
761 patterns. CatBoost and gradient boosting both reached overall accuracy of ap-  
762 proximately 0.80 with similar macro-averaged F1 scores ( $\sim 0.80$ ). For CatBoost,  
763 precision and recall for clean reads were 0.73 and 0.95, respectively, while for  
764 chimeric reads they were 0.92 and 0.66 ( $F1 = 0.77$ ). Gradient boosting showed  
765 nearly identical trade-offs.

766 Random forest attained slightly lower accuracy (0.80) and chimeric F1 (0.76),  
767 whereas logistic regression achieved the lowest accuracy among the four (0.79)  
768 and chimeric F1 (0.74), although it provided the highest chimeric precision (0.95)  
769 at the cost of lower recall (0.61).

770 Across all models, errors were asymmetric. False negatives (chimeric reads  
771 predicted as clean) were more frequent than false positives. For example, CatBoost  
772 misclassified 1 369 chimeric reads as clean but only 215 clean reads as chimeric.  
773 This pattern indicates that the models are conservative: they prioritise avoiding  
774 spurious chimera calls at the expense of missing some true chimeras. Depending on  
775 downstream application, alternative decision thresholds or cost-sensitive training  
776 could be explored to adjust this balance.

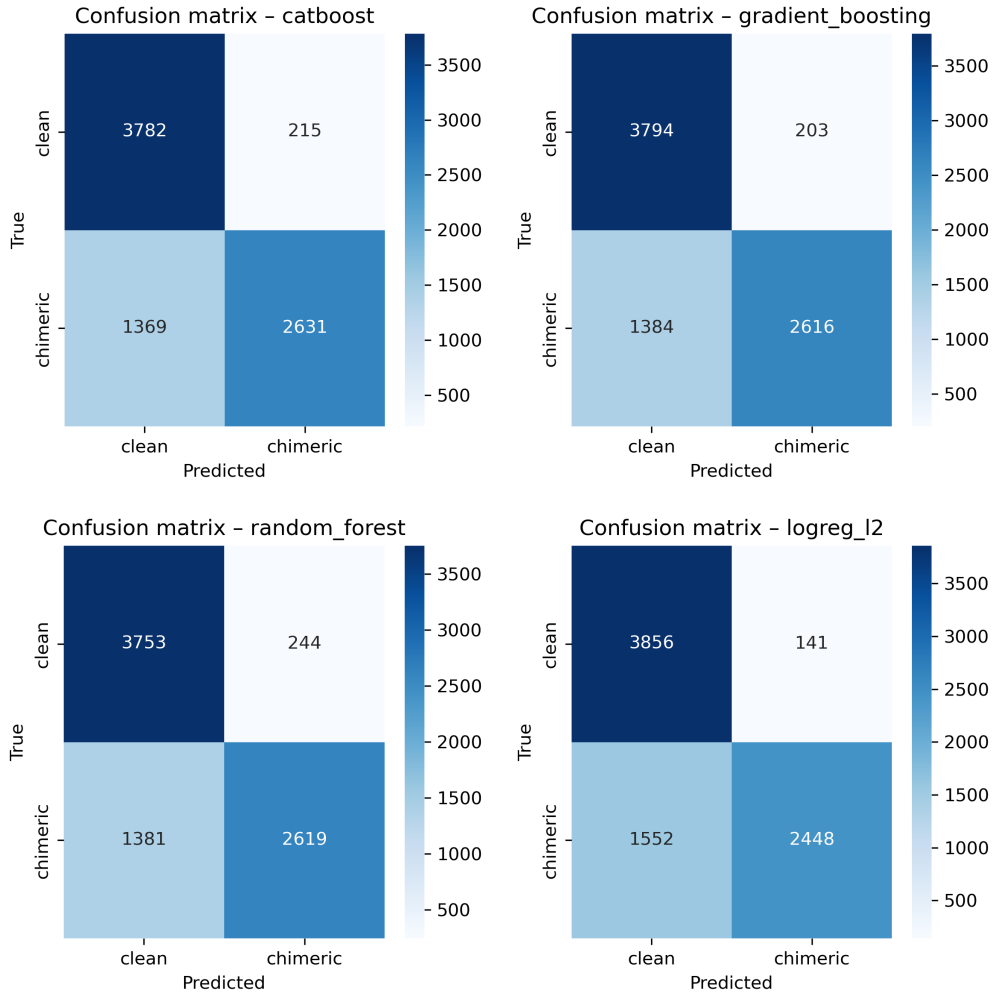


Figure 4.3: Confusion matrices for the four representative models on the held-out test set. All models show more false negatives (chimeric reads called clean) than false positives.

### 4.3.2 ROC and Precision–Recall Curves

778 Receiver operating characteristic (ROC) and precision–recall (PR) curves (Figure 4.4) further support the similarity among the top models. The three tree-based  
 779 ensembles (CatBoost, gradient boosting, random forest) achieved ROC–AUC val-  
 780 ues of approximately 0.84 and average precision (AP) around 0.88. Logistic re-  
 781

782 gression performed slightly worse ( $AUC \approx 0.82$ ,  $AP \approx 0.87$ ) but still substantially  
783 better than random guessing.

784 The PR curves show that precision remains above 0.9 across a broad range  
785 of recall values (up to roughly 0.5–0.6), after which precision gradually declines.  
786 This behaviour indicates that the models can assign very high confidence to a  
787 subset of chimeric reads, while more ambiguous reads can only be recovered by  
788 accepting lower precision.

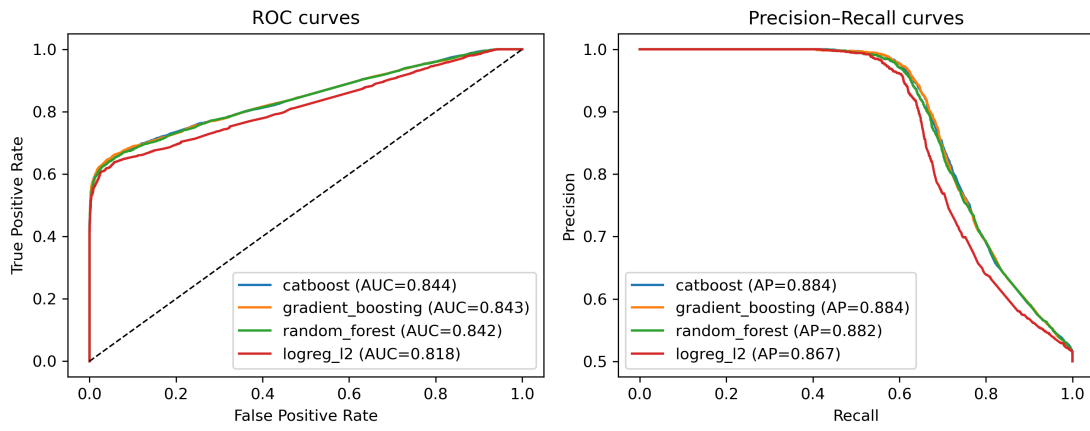


Figure 4.4: ROC (left) and precision–recall (right) curves for the four representative models on the held-out test set. Tree-based ensembles cluster closely, with logistic regression performing slightly but consistently worse.

# <sup>789</sup> References

- <sup>790</sup> Anderson, S., Bankier, A., Barrell, B., Bruijn, M., Coulson, A., Drouin, J., ...  
<sup>791</sup> Young, I. (1981, 04). Sequence and organization of the human mitochondrial  
<sup>792</sup> genome. *Nature*, *290*, 457-465. doi: 10.1038/290457a0
- <sup>793</sup> Arango, G., Garner, E., Pruden, A., Heath, L., Vikesland, P., & Zhang, L. (2018,  
<sup>794</sup> 02). Deeparg: A deep learning approach for predicting antibiotic resistance  
<sup>795</sup> genes from metagenomic data. *Microbiome*, *6*. doi: 10.1186/s40168-018  
<sup>796</sup> -0401-z
- <sup>797</sup> Bentley, D. R., Balasubramanian, S., Swerdlow, H. P., Smith, G. P., Milton, J.,  
<sup>798</sup> Brown, C. G., ... Smith, A. J. (2008). Accurate whole human genome  
<sup>799</sup> sequencing using reversible terminator chemistry. *Nature*, *456*(7218), 53–  
<sup>800</sup> 59. doi: 10.1038/nature07517
- <sup>801</sup> Boore, J. L. (1999). Animal mitochondrial genomes. *Nucleic Acids Research*,  
<sup>802</sup> *27*(8), 1767–1780. doi: 10.1093/nar/27.8.1767
- <sup>803</sup> Cameron, S. L. (2014). Insect mitochondrial genomics: Implications for evolution  
<sup>804</sup> and phylogeny. *Annual Review of Entomology*, *59*, 95–117. doi: 10.1146/  
<sup>805</sup> annurev-ento-011613-162007
- <sup>806</sup> Dierckxsens, N., Mardulyn, P., & Smits, G. (2017). Novoplasty: de novo assembly  
<sup>807</sup> of organelle genomes from whole genome data. *Nucleic Acids Research*,

- 808            45(4), e18. doi: 10.1093/nar/gkw955
- 809    Edgar, R. C. (2016). Uchime2: improved chimera prediction for amplicon se-  
810        quencing. *bioRxiv*. Retrieved from <https://api.semanticscholar.org/>  
811        CorpusID:88955007
- 812    Edgar, R. C. (n.d.). *Uchime in practice*. Retrieved from [https://www.drive5.com/usearch/manual7/uchime\\_practical.html](https://www.drive5.com/usearch/manual7/uchime_practical.html)
- 813    Edgar, R. C., Haas, B. J., Clemente, J. C., Quince, C., & Knight, R. (2011).  
814        Uchime improves sensitivity and speed of chimera detection. *Bioinformatics*,  
815        27(16), 2194–2200. doi: 10.1093/bioinformatics/btr381
- 816    Glenn, T. C. (2011). Field guide to next-generation dna sequencers. *Molecular  
817        Ecology Resources*, 11(5), 759–769. doi: 10.1111/j.1755-0998.2011.03024.x
- 818    Gonzalez, J. M., Zimmermann, J., & Saiz-Jimenez, C. (2004, 09). Evalu-  
819        ating putative chimeric sequences from pcr-amplified products. *Bioin-  
820        formatics*, 21(3), 333-337. Retrieved from <https://doi.org/10.1093/bioinformatics/bti008>  
821        doi: 10.1093/bioinformatics/bti008
- 822    Gray, M. W. (2012). Mitochondrial evolution. *Cold Spring Harbor perspectives  
823        in biology*, 4. Retrieved from <https://doi.org/10.1101/cshperspect.a011403>  
824        doi: 10.1101/cshperspect.a011403
- 825    Hahn, C., Bachmann, L., & Chevreux, B. (2013). Reconstructing mitochondrial  
826        genomes directly from genomic next-generation sequencing reads—a baiting  
827        and iterative mapping approach. *Nucleic Acids Research*, 41(13), e129. doi:  
828        10.1093/nar/gkt371
- 829    Jin, J.-J., Yu, W.-B., Yang, J., Song, Y., dePamphilis, C. W., Yi, T.-S., & Li,  
830        D.-Z. (2020). Getorganelle: a fast and versatile toolkit for accurate de  
831        novo assembly of organelle genomes. *Genome Biology*, 21(1), 241. doi:  
832        10.1186/s13059-020-02154-5  
833

- 834 Judo, M. S. B., Wedel, W. R., & Wilson, B. H. (1998). Stimulation and sup-  
835 pression of pcr-mediated recombination. *Nucleic Acids Research*, *26*(7),  
836 1819–1825. doi: 10.1093/nar/26.7.1819
- 837 Labrador, K., Agmata, A., Palermo, J. D., Ravago-Gotanco, R., & Pante, M. J.  
838 (2021). Mitochondrial dna reveals genetically structured haplogroups of  
839 bali sardinella (sardinella lemuru) in philippine waters. *Regional Studies in*  
840 *Marine Science*, *41*, 101588. doi: 10.1016/j.rsma.2020.101588
- 841 Layer, R., Hall, I., & Quinlan, A. (2014, 10). Lumpy: A probabilistic framework  
842 for structural variant discovery. *Genome Biology*, *15*. doi: 10.1186/gb-2014  
843 -15-6-r84
- 844 Li, H. (2018, 05). Minimap2: pairwise alignment for nucleotide sequences. *Bioin-*  
845 *formatics*, *34*(18), 3094-3100. Retrieved from <https://doi.org/10.1093/bioinformatics/bty191> doi: 10.1093/bioinformatics/bty191
- 846 Liang, Q., Bible, P. W., Liu, Y., Zou, B., & Wei, L. (2020, 02). Deepmi-  
847 crobes: taxonomic classification for metagenomics with deep learning. *NAR*  
848 *Genomics and Bioinformatics*, *2*(1), lqaa009. Retrieved from <https://doi.org/10.1093/nargab/lqaa009> doi: 10.1093/nargab/lqaa009
- 849 Metzker, M. L. (2010). Sequencing technologies — the next generation. *Nature*  
850 *Reviews Genetics*, *11*(1), 31–46. doi: 10.1038/nrg2626
- 851 Mysara, M., Saeys, Y., Leys, N., Raes, J., & Monsieurs, P. (2015). Catch,  
852 an ensemble classifier for chimera detection in 16s rrna sequencing stud-  
853 ies. *Applied and Environmental Microbiology*, *81*(5), 1573-1584. Retrieved  
854 from <https://journals.asm.org/doi/abs/10.1128/aem.02896-14> doi:  
855 10.1128/AEM.02896-14
- 856 Peccoud, J., Lequime, S., Moltini-Conclois, I., Giraud, I., Lambrechts, L., &  
857 Gilbert, C. (2018, 04). A survey of virus recombination uncovers canon-

- 860       ical features of artificial chimeras generated during deep sequencing li-  
861       brary preparation. *G3 Genes—Genomes—Genetics*, 8(4), 1129-1138. Re-  
862       trieved from <https://doi.org/10.1534/g3.117.300468> doi: 10.1534/  
863       g3.117.300468
- 864       Qin, Y., Wu, L., Zhang, Q., Wen, C., Nostrand, J. D. V., Ning, D., ... Zhou, J.  
865       (2023). Effects of error, chimera, bias, and gc content on the accuracy of  
866       amplicon sequencing. *mSystems*, 8(6), e01025-23. Retrieved from <https://journals.asm.org/doi/abs/10.1128/msystems.01025-23> doi: 10.1128/  
867       msystems.01025-23
- 868       Qiu, X., Wu, L., Huang, H., McDonel, P. E., Palumbo, A. V., Tiedje, J. M., &  
869       Zhou, J. (2001). Evaluation of pcr-generated chimeras, mutations, and het-  
870       eroduplexes with 16s rrna gene-based cloning. *Applied and Environmental  
871       Microbiology*, 67(2), 880–887. doi: 10.1128/AEM.67.2.880-887.2001
- 872       Ren, J., Song, K., Deng, C., Ahlgren, N., Fuhrman, J., Li, Y., ... Sun, F. (2020,  
873       01). Identifying viruses from metagenomic data using deep learning. *Quan-  
874       titative Biology*, 8. doi: 10.1007/s40484-019-0187-4
- 875       Rodriguez-Martin, B., Palumbo, E., Marco-Sola, S., Griebel, T., Ribeca, P.,  
876       Alonso, G., ... Djebali, S. (2017, 01). Chimpipe: Accurate detection of  
877       fusion genes and transcription-induced chimeras from rna-seq data. *BMC  
878       Genomics*, 18. doi: 10.1186/s12864-016-3404-9
- 879       Rognes, T., Flouri, T., Nichols, B., Quince, C., & Mahé, F. (2016). Vsearch: a  
880       versatile open source tool for metagenomics. *PeerJ*, 4, e2584. doi: 10.7717/  
881       peerj.2584
- 882       Sedlazeck, F., Rescheneder, P., Smolka, M., Fang, H., Nattestad, M., von Haeseler,  
883       A., & Schatz, M. (2018, 06). Accurate detection of complex structural  
884       variations using single-molecule sequencing. *Nature Methods*, 15. doi: 10  
885

- 886 .1038/s41592-018-0001-7
- 887 Sfeir, A., & Symington, L. S. (2015). Microhomology-mediated end joining: A  
888 back-up survival mechanism or dedicated pathway? *Trends in Biochemical  
889 Sciences*, 40(11), 701-714. Retrieved from <https://www.sciencedirect.com/science/article/pii/S0968000415001589> doi: <https://doi.org/10.1016/j.tibs.2015.08.006>
- 890
- 891
- 892 Vervier, K., Mahé, P., Tournoud, M., Veyrieras, J.-B., & Vert, J.-P. (2015,  
893 11). Large-scale machine learning for metagenomics sequence classifica-  
894 tion. *Bioinformatics*, 32(7), 1023-1032. Retrieved from <https://doi.org/10.1093/bioinformatics/btv683> doi: 10.1093/bioinformatics/btv683
- 895
- 896 Willette, D., Bognot, E., Mutia, M. T., & Santos, M. (2011). *Biology and ecology  
897 of sardines in the philippines: A review* (Vol. 13; Tech. Rep. No. 1). NFRDI  
898 Technical Paper Series. Retrieved from <https://nfrdi.da.gov.ph/tpjf/etc/Willette%20et%20al.%20Sardines%20Review.pdf>
- 899